COBEM 2025
28TH INTERNATIONAL CONGRESS OF MECHANICAL ENGINEERING
ABCM Brazilian Society of Mechanical Sciences and Engineering
28th ABCM International Congress of Mechanical Engineering
November 09-11, 2025, Curitiba-PR, Brazil

COB-2025-0308
THERMAL OPTIMIZATION IN MACHINING VIA INVERSE HEAT CONDUCTION

Rogério Fernandes Brito
Vinicius Gonçalves Pereira
Ruben Alexis Miranda Carrillo
Paulo Mohallem Guimarães
Ricardo Luiz Perez Teixeira
José Carlos de Lacerda
Tarcísio Gonçalves de Brito
Fábio Santos Nascimento
Federal University of Itajubá, UNIFEI, Theodomiro Carneiro Santiago Campus – Itabira, Irmã Ivone Drumond, St. #200 – Distrito Industrial II, Zip code: 35,903-087, Itabira – MG – Brazil.
rogbrito@unifei.edu.br; d2022002883@unifei.edu.br; ruben.miranda@unifei.edu.br; pauloguimaraes@unifei.edu.br; ricardo.luiz@unifei.edu.br; jlacerda@unifei.edu.br; tgbrito@unifei.edu.br; fabiosn@unifei.edu.br

Solidônio Rodrigues de Carvalho
College of Mechanical Engineering, Federal University of Uberlândia, UFU, Santa Monica Campus, Avenida Joao Naves de ´Avila 2121, Zip code: 38,408-100, Uberlândia, MG, Brazil.
solidonio@ufu.br

Sandro Metrevelle Marcondes de Lima E Silva
Federal University of Itajubá, UNIFEI, Prof. José Rodrigues Seabra Campus – Headquarters, BPS, Av. #1303, Pinheirinho district, ZIP code: 37,500 903, Itajubá – MG – Brazil.
metrevel@unifei.edu.br

Júlio César Costa Campos
Henrique Marcio Pereira Rosa
Department of Production and Mechanical Engineering - DEP, Laboratory of Thermal Systems - LST, Federal University of Viçosa - UFV, Zip code: 36,570-900, Viçosa, MG, Brazil.
julio.campos@ufv.br; henrique.rosa@ufv.br

Elisan dos Santos Magalhaes
Technological Institute of Aeronautics (ITA), Division of Mechanical Engineering, Department of Energy, Praça Marechal Eduardo Gomes, #50, Zip code: 12,228-900, São José dos Campos, SP, Brazil.
elisan@ita.br

Abstract. *The effect of cutting parameters—workpiece rotation speed, depth of cut, and feed rate—on the temperature distribution across the rake face of an AISI M32C high-speed steel cutting tool is analyzed. The study focuses on machining ABNT 12L14 steel to evaluate thermal behavior under different cutting conditions. Using COMSOL® Multiphysics 6.0 for 3D transient heat transfer modeling, three inverse methods—Levenberg-Marquardt, Linear Specified Function, and Nelder-Mead—to estimate heat flux at the chip-tool interface were implemented. Our results show that the Levenberg-Marquardt method achieves the best accuracy, with estimated temperatures deviating by as little as 1.5% from experimental data. This study highlights the effectiveness of optimized cutting parameters in minimizing tool temperature and extending tool life, with the proposed method offering practical benefits for industrial machining processes.*

Keywords: *heat transfer, inverse methods, Levenberg-Marquardt, linear specified function, Nelder-Mead.*

1. INTRODUCTION

Temperature control is crucial in machining, affecting tool performance, wear resistance, and surface quality. Excessive heat at the chip-tool interface accelerates tool wear, reduces productivity, and raises costs. Accurate temperature estimation and heat management are vital for process optimization and tool longevity (Trent *et al*., 2025; Brito *et al*., 2015). This study analyzes the effect of cutting parameters on tool temperature and uses inverse heat conduction to estimate temperatures at the tool-workpiece interface.

Measuring temperature in machining is difficult due to localized, fast-changing heat at the interface (Brito *et al*., 2009; D'Addona and Raykar, 2019). Techniques like thermocouples and infrared cameras have limitations in measuring exact contact points (Brito *et al*., 2015). Inverse methods overcome this by estimating temperature and heat flux from nearby measurements, improving prediction accuracy (Machado *et al*., 2015; Carvalho *et al*., 2006). Santos *et al*. (2014) showed that, for convection coefficients (h) from 10–30 W/m²·K, the impact on interface temperature was under 0.74 %, justifying the use of h = 20 W/m²·K. Simulations included temperature-dependent material properties, with tool temperatures ranged from 160 °C to 570 °C.

Common measurement tools include embedded thermocouples, infrared cameras, and TFTCs, offering insights into heat and tool wear but challenged by placement and response time issues (Chen *et al*., 2017; Soler *et al.,* 2018). K-type thermocouples, with ± 2 °C accuracy, were used by Chen *et al*. (2017), while Soler *et al.* (2018) used infrared cameras for better precision. Despite advances, experimental limits demand integration with numerical modeling.

Thermal issues in machining require analytical, numerical, and inverse approaches. Analytical models suit simpler cases but involve simplifications (Kashani *et al*., 2016). Finite Element Analysis (FEA) enables detailed simulations of complex geometries but is computationally expensive (Clavier *et al*., 2021). Inverse methods like Levenberg-Marquardt and Nelder-Mead enhance thermal property estimation (Dourado da Silva *et al*., 2021). This study uses COMSOL® Multiphysics to apply these techniques and optimize cutting conditions (COMSOL, 2018). FEA allows flexible meshing and complex boundary conditions (Thornton and Wieting, 1979). COMSOL's transient heat transfer module employs a second-order backward differentiation formula (BDF) for time discretization and PARDISO solvers for efficient sparse matrix solutions (COMSOL, 2018; PARDISO-PROJECT, 2019).

The main objective of this work is to investigate the effect of cutting parameters - workpiece rotation speed, depth of cut, and feed rate - on the thermal behavior of a high-speed steel tool during the machining of ABNT 12L14 steel. The study aims to estimate the heat flux at the chip-tool interface using inverse techniques and to evaluate the accuracy and performance of Levenberg-Marquardt, Linear Specified Function, and Nelder-Mead methods. The results are intended to contribute to thermal optimization strategies in machining processes and enhance tool life by improving temperature prediction and control.

2. METHODOLOGY

This study builds upon the experimental work of Santos *et al*. (2014). The main machining experiments involved turning AISI 12L14 free-machining steel (Ø 50.8 mm), heat-treated to Rockwell B 68 with a ferritic microstructure, using a Revolution RV220 Diplomat lathe and an AISI M32C high-speed steel tool. These properties were essential to evaluate tool performance and thermal response under varying cutting conditions (detailed in Section 2.1). Validating inverse heat conduction methods is challenging due to unknown experimental heat flux in real-world machining. To address this, a separate controlled validation experiment, originally performed by Carvalho *et al*. (2006) and referenced by Santos *et al*. (2014), was used. This validation setup employed a cemented carbide tool (0.0127 m × 0.0127 m × 0.0047 m), a Kapton electric heater, a heat flux transducer, two calibrated thermocouples, and thermal paste for optimized contact (Figure 1). Data were acquired using an HP 75000 system and E1326B voltmeter. Using this controlled setup, numerical simulations in COMSOL® were validated by comparing simulation results (using inverse methods fed with thermocouple data) against the measured heat flux from the transducer. The heater generated heat via the Joule effect, and the transducer measured the heat reaching the tool base. Temperature readings were collected at two points (*T01*, *T02*) for inverse problem analysis.

The direct heat transfer problem (calculating temperature from known heat flux) was solved using COMSOL's Finite Element Method (FEM). The inverse problem (estimating heat flux from known temperature measurements) was approached using the temperature data from the validation experiment and three optimization methods: Nelder-Mead (NM), Levenberg-Marquardt (LM), and Linearly Specified Function (LSF). The LM method yielded the best balance between accuracy and computational cost in this validation phase. Finally, the validated inverse techniques, primarily the LM method implemented in COMSOL®, were applied to analyze the main experiments involving the turning of free-machining steel with the high-speed steel tool under the various cutting conditions outlined in Section 2.1.

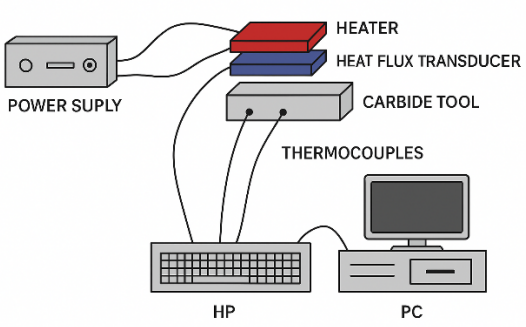

Figure 1. Schematic of the experimental set-up made by Carvalho *et al.* (2006). Source: Santos *et al*. (2014).

2.1. ANALYTICAL, NUMERICAL, AND INVERSE TECHNIQUES FOR SOLVING THERMAL PROBLEM

The methodology focuses on estimating heat flux on the rake face of the AISI M32C high-speed steel cutting tool during turning, based on experimental temperature measurements at specific points within the tool. The analysis centers on the cutting interface, as illustrated in the CAD drawings Figure 2 corresponding to Case 1 from the experiments conducted by Santos *et al.* (2014). The cutting parameters for all cases are listed in Tab. 1.

Table 1. Description of the cutting parameters for each case addressed in this work.

Case	Cutting speed (m/min)	Depth of cut (mm)	Feed rate (mm/rev)	Contact area (mm^2)	Perimeter of Contact Area (mm)
1	143	1.0	0.138	1.46	4.8
2	57	1.0	0.138	0.75	3.88
3	57	2.0	0.138	1.56	5.77
4	57	1.0	0.298	1.64	4.74
5	5	1.0	0.138	0.64	3.36

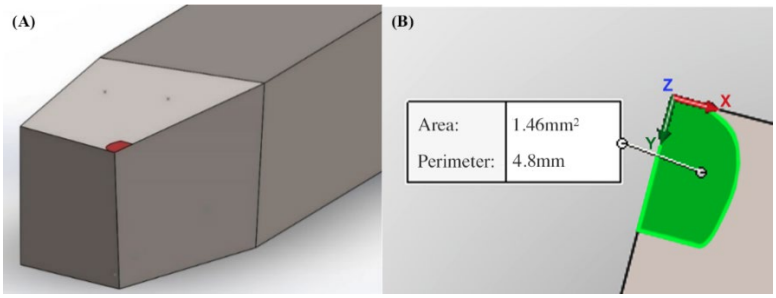

Figure 2. a) High-speed steel cutting tool for Case 1; b) Zoomed wear region. (Source: Adapted from Santos *et al*., 2014).

The contact area was determined post-interruption by averaging measurements from three distinct tool edges for each condition using an image processing system (GLOBAL LABÒ Image software) with a high-resolution video camera (Santos *et al*., 2014). According to Dourado da Silva *et al.* (2021), Santos *et al*. (2014), and Lian Y *et al.* (2023), the thermal analysis focuses on the tool's rake face (Figures 3 and 4), where the wear region generates the most heat flux.

Figure 3(a) shows the experimental setup from Santos et al. (2014) using a conventional IMOR MAXI - II - 520 – 6 cv lathe. T-type thermocouples were attached via capacitive discharge. Data acquisition used an HP 75000 Series B system with an E1326B voltmeter. Figure 3(b) shows the 3D model, and 3(c) its dimensions.

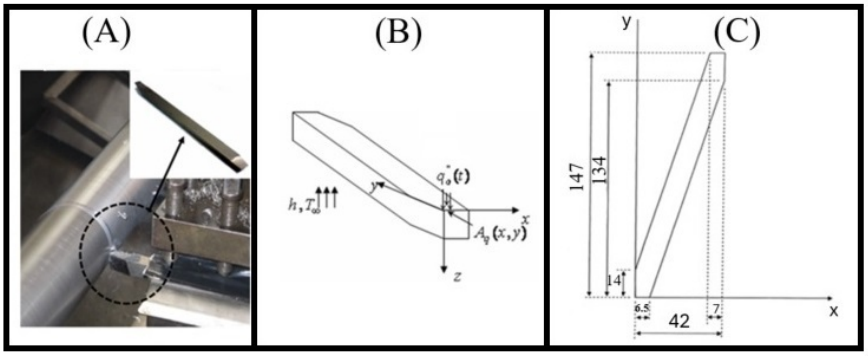

Figure 3. (a) High-speed steel tool, (b) three-dimensional physical model, and (c) tool dimensions in millimeters (mm) where the coordinate "*z*" is 9.5 (mm). Source: Santos *et al*. (2014).

Heat flux estimation depends critically on thermocouple locations. The heat flux $q''(x, y, t)$ occurs at the interface contact area $A_q(x, y)$. A constant convective heat transfer coefficient h = 20 W/m²·K is assumed on other boundaries (Nosko, 2024). Figure 4 shows the thermocouple positions used by Santos *et al.* (2014).

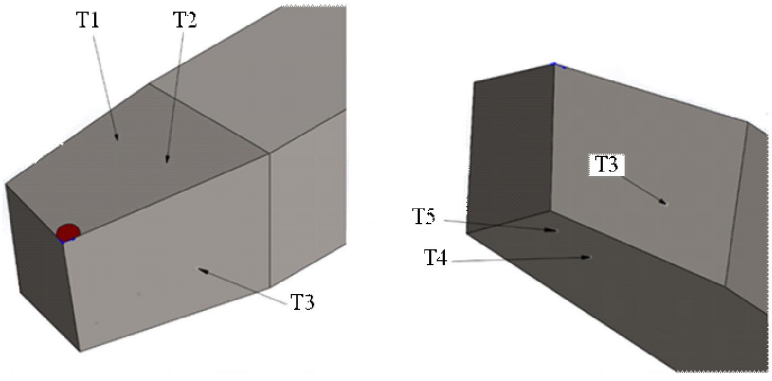

Figure 4. Position of the thermocouples on the high-speed steel cutting tool. (Source: Adapted from Santos *et al.,* 2014).

The specific thermocouple positions were: - Thermocouple 1: X = 6.1 mm; Y = 7.2 mm; Z = 0.0 mm; - Thermocouple 3: X = 0.0 mm; Y = 9.0 mm; Z = 5.0 mm; - Thermocouple 4: X = 3.3 mm; Y = 7.0 mm; Z = 8.098 mm; and - Thermocouple 5: X = 2.0 mm; Y = 3.4 mm; Z = 8.098 mm.

The AISI M32C high-speed steel tool specifications were: rake angle: 6°; approach angle: 75°; inclination angle: 0°; nose angle: 90°; relief angle: 8°; nose radius: none. The thermal problem is governed by the 3D transient heat diffusion equation (Eq. 1), where T is temperature, λ is thermal conductivity, and $\rho\, c_p$ is the product of density and specific heat capacity (Santos *et al.,* 2014).

$$\frac{\partial}{\partial x}\left(\lambda\frac{\partial T}{\partial x}\right)+\frac{\partial}{\partial y}\left(\lambda\frac{\partial T}{\partial y}\right)+\frac{\partial}{\partial z}\left(\lambda\frac{\partial T}{\partial z}\right)=\rho c_p\frac{\partial T}{\partial t} \tag{1}$$

COMSOL Multiphysics 6.0 (COMSOL, 2018) was used for FEM solutions to direct and inverse problems, employing an unstructured tetrahedral mesh Figure 5(a), both for the case studied and for the case of validation using the controlled experiment (Santos *et al*., 2014).

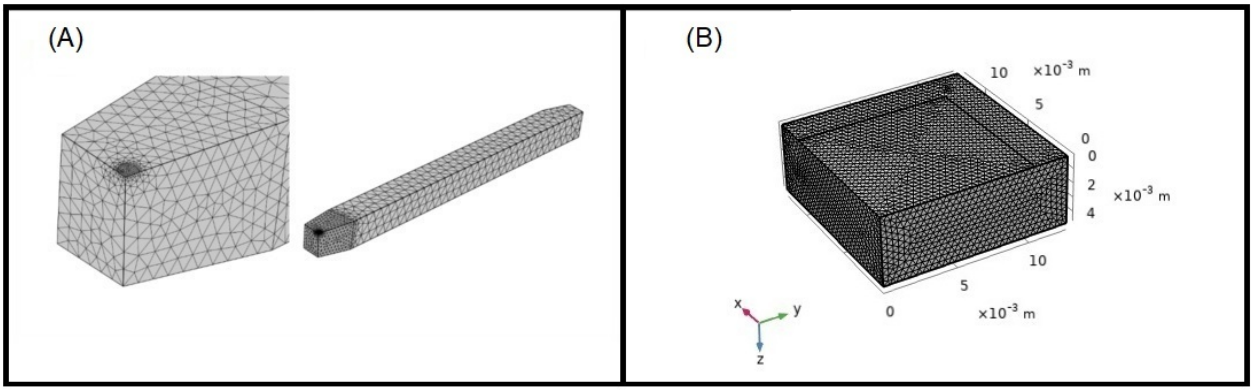

Figure 5. Cutting tool domain: (A) with tetrahedral mesh (6,952 elements, Case 4); (B) mesh applied to the cemented carbide tool, for validating the direct heat transfer problem (143,908 elements).

The mesh Figure 5(b) for the validation problem (cemented carbide tool) was automatically sized by COMSOL. For the main HSS tool simulations, a mesh convergence study (Section 3.3) determined that a mesh with approximately 6,952 tetrahedral elements (Figure 5a), shown for Case 4 offered a good balance between accuracy and computational cost. Tetrahedral meshes adapt well to complex geometries.

The inverse problem aims to estimate the transient heat flux $q''(x,y,t)$ that minimizes the discrepancy between numerically calculated temperatures (T_{num}) and experimental measurements (T_{exp}) at sensor locations. Three optimization techniques were evaluated: Levenberg-Marquardt (LM), Nelder-Mead (NM), and Linear Specified Function (LSF).

- Levenberg-Marquardt (LM): Combines gradient-descent and Gauss-Newton methods, using Jacobian matrix information. Efficient for smooth, differentiable functions (Levenberg, 1944; Marquardt, 1963).
- Nelder-Mead (NM): A gradient-free direct search method using simplex geometry. Robust for noisy or discontinuous functions but can be computationally expensive (Nelder and Mead, 1965).
- Linear Specified Function (LSF): Iteratively approximates parameters using piecewise linear functions. Can reduce sensitivity to noise (Beck *et al*., 1985).

The objective function adopted from Lima e Silva *et al*. (2015) minimizes the sum of squared differences between experimental and numerical temperatures (Eq. 2):

$$F = \sum_{i=1}^{ns}(T_{exp}(x,y,z,t)_p - T_{num}(x,y,z,t)_p)^2, \quad (2)$$

where F is the objective function, ns is the number of sensors, N is the number of time steps, and p is the sensor index.

3. RESULTS AND DISCUSSION

The validation used the controlled experiment with the cemented carbide tool (Figure 5b). Experimental temperatures *T01* and *T02* were input into the LM, LSF, and NM inverse algorithms within COMSOL® to estimate the heat flux applied by the heater. These estimated fluxes were then compared to the experimentally measured flux from the transducer (Figure 6). Figures 6(a) and 6(b) compare the temperatures calculated using these estimated fluxes against the experimental temperatures measured by thermocouples *T01* and *T02*.

Figure 7 presents the results of the numerical temperatures estimated against the experimental temperatures obtained in the work by Santos *et al*., (2014). There was good agreement between them.

Figure 8 shows the temperature residuals (difference between numerical and experimental) for the LM and LSF methods. NM residuals are omitted due to excessive computation time needed for stable results. The residuals for LM and LSF remain below 3°C during the effective period.

Computational cost was a key factor Tab. 2. The NM method was significantly slower, making it impractical for the subsequent analyses.

Considering the accuracy (Figures 6, 7, 8) and computational efficiency Tab. 2, the Levenberg-Marquardt (LM) method was selected as the most suitable. An additional advantage is that LM can be implemented entirely within COMSOL. LSF required integration between MATLAB® (for the algorithm) and COMSOL® (for the FEM solver), adding complexity.

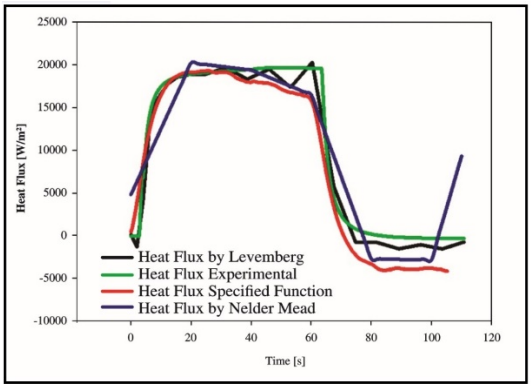

Figure 6. Comparison of experimental heat flux and heat flux estimated by LSF, LM, and NM techniques during the validation experiment (heater active up to 63.27 s).

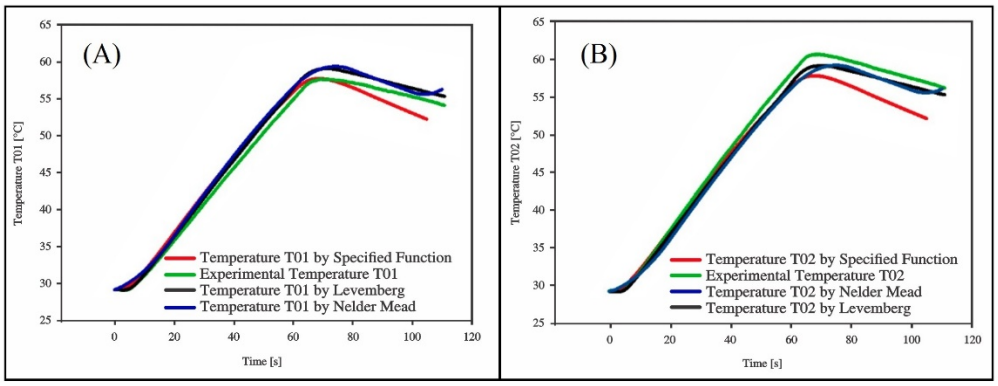

Figure 7. Comparison of numerical temperatures (calculated using estimated fluxes from each technique) and experimental temperatures for the validation experiment: a) Thermocouple *T01*; b) Thermocouple *T02*.

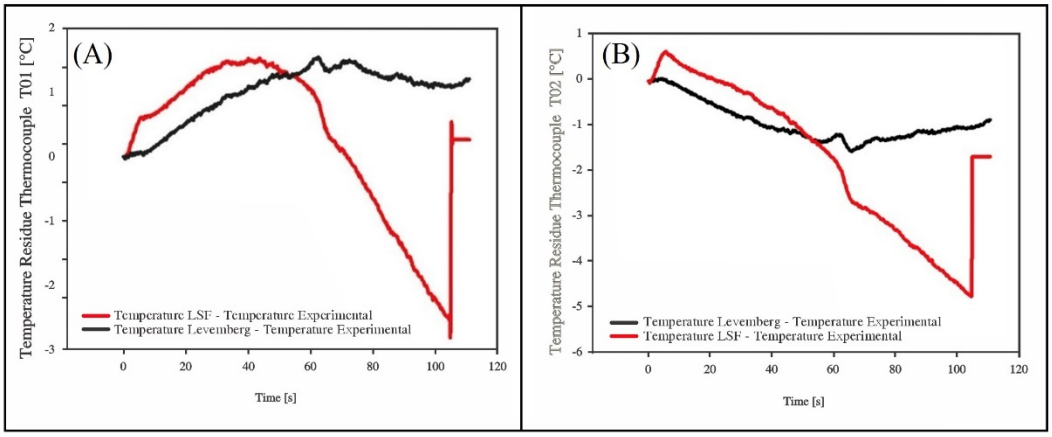

Figure 8. Residual temperature between LM and LSF regarding experimental data for: a) Thermocouple *T01*; b) Thermocouple *T02*.

Table 2. Computational Time spent solving the inverse problem by each technique.

Ranking	Inverse Technique	Computational Time Spent [min]
1º	Levenberg-Marquardt	~5
2º	Linear Specified Function	~5
3º	Nelder-Mead	4,441

3.1 HEAT FLUX AND TEMPERATURE ESTIMATION USING LEVENBERG-MARQUARDT (MACHINING CASES)

The LM method was applied to estimate heat flux and temperature distribution for the five machining cases (Table 1) using the experimental temperature data (from thermocouples *T01*, *T03*, *T04*, *T05* - note *T01* was used here but *T03* in the mesh study, confirm which were primary) measured by Santos et al. (2014) on the AISI M32C HSS tool. The COMSOL model used the geometry from Figure 3(b) and the mesh configuration determined in Section 3.3. The temporal discretization matched the experiment (0.112 s interval). Total experiment duration varied (e.g., 126.224 s for Case 1, 87.248 s for Case 4). Experiments started at room temperature (~25°C) with natural air convection cooling.

3.2 FINITE ELEMENTS MESH CONFIGURATION STUDY FOR LEVENBERG-MARQUARDT TECHNIQUE

A mesh convergence study was performed using Case 4 data on a computer with an Intel® Xeon W-1250 (3.30 GHz), 64 GB RAM. Different tetrahedral mesh densities (ranging from 2,564 to 42,388 elements) were tested, evaluating computational time and the maximum percentage deviation between numerical (LM estimated) and experimental temperatures (from Santos *et al*., 2014) for thermocouples *T03*, *T04*, and *T05*.

The results indicated a substantial increase in computational time as the number of finite elements grew. A coarse mesh of 2,564 elements required approximately 15 minutes to process, while the finest mesh tested, with 42,388 elements, took over 10 hours. Intermediate meshes showed progressively longer times: 3,180 elements required 21 minutes, 6,952 took 38 minutes, 9,351 took 1 hour and 11 minutes, and 12,541 required 1 hour and 32 minutes.

Although computational effort increased significantly, the accuracy remained nearly constant across all mesh sizes. The maximum percentage deviations between the numerical and experimental temperatures were quite stable. For thermocouple T03, deviations ranged narrowly from 2.1375% to 2.1592%; for *T04*, from 1.3805% to 1.4047%; and for T05, from 0.5840% to 0.6018%. These values suggest that even the coarser meshes produced results close to the converged solution.

This behavior highlights that beyond a certain mesh density—approximately 7,000 to 9,000 elements—further refinement offers minimal gains in accuracy while substantially increasing computational cost. Therefore, a moderate mesh density provides a more efficient balance between solution precision and processing time for similar simulations.

The results indicate that increasing mesh density beyond ~6,952 elements yielded diminishing returns in accuracy while significantly increasing computational time. The mesh with 6,952 elements provided accuracy comparable to the finest mesh (42,388 elements) but was approximately 17 times faster. Therefore, this mesh density was selected for simulating all five cases.

3.3 RESULTS CORRESPONDING TO CASE 1 – 900 RPM, 1.0 MM DEPTH OF CUT AND 0.138 MM/REV FEED RATE

Figure 10 (a) compares the heat flux estimated using the LM method in this study with the estimation by Santos *et al*. (2014) (who used an "Inverse 3D technique" likely similar to LSF). Figure 10 (b) shows the percentage deviation between the two estimations.

Good agreement is observed, especially during the effective cutting period (up to ~50 s). The deviation increases after the tool disengages.

Figure 11 shows the agreement between the numerical and experimental temperatures for Case 1 is excellent. The percentage deviation over time remains low for all thermocouples evaluated. Thermocouple *T01* shows deviations that stay mostly within ±1%, while *T04* exhibits a slightly higher deviation, peaking at around 1.5% before gradually decreasing. Thermocouple *T05* presents the most stable behavior, with deviations generally remaining below ±0.5%. These results demonstrate a strong correlation between the simulated temperatures obtained using the Levenberg–Marquardt method and the experimental measurements, validating the accuracy of the numerical model.

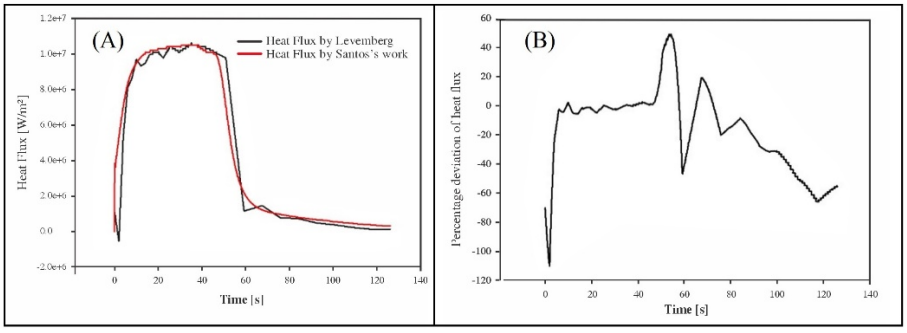

Figure 10. Case 1: a) Comparison between heat flux estimated by Levenberg-Marquardt (this study) and flux estimated by Santos *et al.* (2014); b) Percentage deviation between the two estimated fluxes.

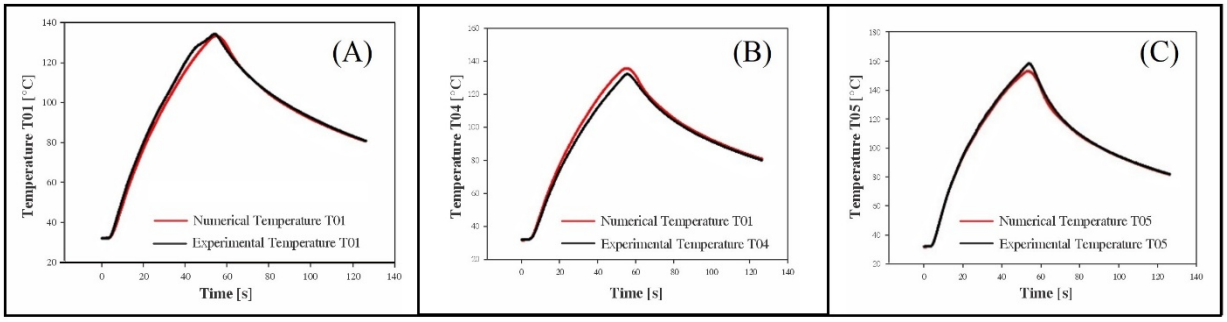

Figure 11. Case 1: Comparison between numerical temperatures (Levenberg-Marquardt) and experimental temperatures (Santos *et al*., 2014). a) Thermocouple *T01*; b) Thermocouple *T04*; c) Thermocouple *T05*.

The maximum deviation remained below 1.5%, validating the LM method's effectiveness even for this high-speed case. Figure 12 illustrates the calculated temperature field evolution on the cutting tool at different time points.

The calculated maximum, average, and minimum temperatures within the wear region—identified previously—were estimated over time. This area is not accessible to direct measurement due to the continuous contact between the tool and chip. The temperature profile shows a rapid increase at the beginning of the process, with maximum temperatures reaching approximately 600 °C, followed by average and minimum values that remain consistently lower. After peaking, all temperature values begin to gradually decrease, reflecting the thermal behavior in the wear region as cutting progresses and heat dissipates.

This provides valuable insight into the thermal conditions experienced by the most critical part of the tool during machining.

3.4 COMPARISON OF STUDIED CASES

Simulations were performed for all five cases using the LM method. The key thermal findings for the wear region temperatures were: - Case 1 (900 RPM, Depth of Cut: 1.0 mm, Feed Rate: 0.138 mm/rev): i) This scenario exhibits the highest temperatures in the tool wear region, exceeding 570 °C; - The elevated rotational speed (900 RPM) significantly increases heat generation at the cutting interface, resulting in higher thermal gradients and substantial heat dissipation. - Case 2 (355 RPM, Depth of Cut: 1.0 mm, Feed Rate: 0.138 mm/rev): i) Reducing the rotational speed decreased heat generation, leading to maximum temperatures around 400 °C; ii) This case demonstrates a marked reduction in thermal impact compared to Case 1, highlighting the influence of rotational speed on heat generation. - Case 3 (355 RPM, Depth of Cut: 1.0 mm, Feed Rate: 0.298 mm/rev): i) Increasing the feed rate to 0.298 mm/rev intensifies heat generation, raising the maximum temperature to approximately 537 °C; ii) The more aggressive material removal due to the higher feed rate is the primary contributor to the observed increase in temperature. - Case 4 (355 RPM, Depth of Cut: 2.0 mm, Feed Rate: 0.138 mm/rev): i) A greater depth of cut (2.0 mm) leads to slightly higher temperatures, with a peak of 461.2 °C, compared to Case 2; ii) This results highlights the role of the depth of cut in affecting heat dissipation through the cutting tool. -

Case 5 (28 RPM, Depth of Cut: 1.0 mm, Feed Rate: 0.138 mm/rev): i) The low rotational speed significantly reduces heat generation, with maximum temperatures not exceeding 160 °C; ii) This configuration results in the lowest thermal gradients, reflecting the effect of a less severe cutting condition.

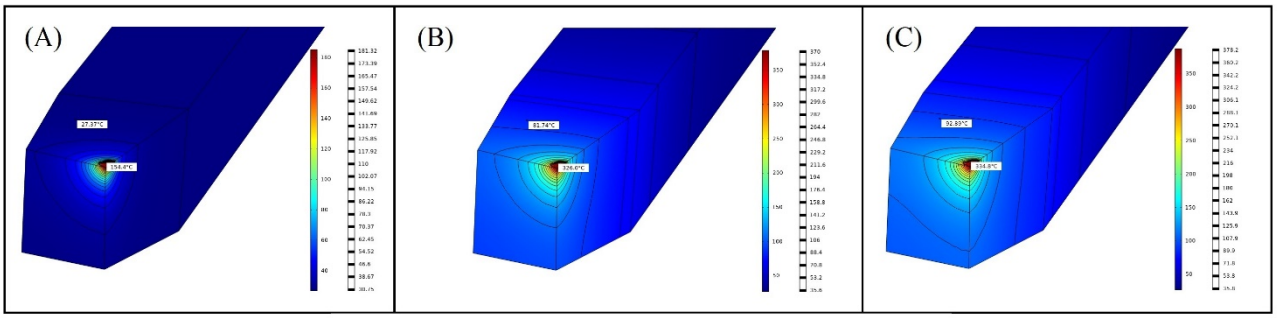

Figure 12. Case 1: Temperature field on the cutting tool estimated by the LM model: a) t = 5 s; b) t = 50 s (peak cutting); c) t = 85 s (cooling). At t = 50 s, significant thermal gradients are visible, with peak temperatures exceeding 570 °C near the cutting edge.

3.5 IMPACT OF CUTTING PARAMETERS

The results confirm the significant influence of cutting parameters on tool temperature: - Rotational Speed (Cutting Speed): Has the most dominant effect. Higher speeds lead to exponentially higher interface temperatures due to increased friction and shear energy per unit time; - Feed Rate: Increasing feed rate increases the material removal rate and associated heat generation, leading to higher temperatures (compare Case 4 vs. Case 2); - Depth of Cut: Increasing depth of cut increases the contact area and volume of deformed material, leading to higher heat generation, though its impact seemed less pronounced than speed or feed rate in the ranges studied (compare Case 3 vs. Case 2).

Optimizing these parameters is crucial for managing tool temperature, reducing wear, and extending tool life.

4. CONCLUSIONS

Successful validation of the inverse methods, with the Levenberg-Marquardt (LM) method demonstrating the best balance between accuracy and computational cost. Application of the LM method to estimate heat flux and temperature in five machining cases involving ABNT 12L14 steel with an AISI M32C high-speed steel tool. Excellent agreement (<1.5% deviation) was found between temperatures estimated by the LM method and the experimental data from Santos et al. (2014). Quantification of the impact of parameters showed that cutting speed has the most significant effect, followed by feed rate and depth of cut. Maximum temperatures in the wear region ranged from approximately 160 °C (Case 5) to over 570 °C (Case 1), highlighting the importance of cutting parameter control. The proposed methodology (FEM + LM) is an effective tool for thermal analysis in machining and process optimization. Future work should address limitations such as the dependence on experimental accuracy and the assumption of a constant heat transfer coefficient. It may also include wear modeling and more complex geometries (e.g., including wear models, more complex geometries).

5. ACKNOWLEDGMENTS

The Minas Gerais State Research Foundation (FAPEMIG) supported the work, Process No. APQ-02317-18 - Reg.: 42/2019, titled “Application of Inverse Problem Techniques for the Thermal Study of Machining Tools with Different Geometries and Coatings”.

6. REFERENCES

Beck, J.V., Blackwell, B. and St. Clair, C., 1985. *Inverse Heat Conduction: Ill-posed Problems*. Wiley-Interscience Publication: New York.

Brito, R.F., Carvalho S.R. and Ferreira J.R., 2009. “Thermal analysis in coated cutting tools”. *Int. Commun. Heat Mass Transfer*, Vol. 36(4), pp. 314-321. https://doi.org/10.1016/j.icheatmasstransfer.2009.01.009

Brito R.F., Carvalho, S.R. and Lima e Silva, S.M.M., 2015. "Experimental investigation of thermal aspects in a cutting tool using COMSOL and inverse problem". *Appl. Therm. Eng*., Vol. 86, pp. 60-68. https://doi.org/10.1016/j.applthermaleng.2015.03.083

Carvalho, S.R., Lima e Silva, S.M.M., Machado, A.R. and Guimarães, G. 2006. "Temperature determination at the chip-tool interface using an inverse thermal model considering the tool and tool holder". *J. Mater. Process. Technol*., Vol. 179, pp. 97-104.

Chen, L., Tai, B.L., Chaudhari, R.G., Song, X. and Shih, A.J. 2017. "Machined Surface Temperature in Hard Turning", *Int. J. of Machine Tools and Manufacture*. Vol. 121, pp. 10-21. https://doi.org/10.1016/j.ijmachtools.2017.03.003

Clavier. F., Valiorgue, F., Courbon, C., Rech, J., Van, R.A., Mascitonio, U., Brosse, A. and Dorlin, T. 2021. "Numerical analysis of the tribological and geometrical impacts of tool wear on the thermomechanical loadings induced by 15-5PH steel turning". In. *Proc. CIRP 2021*, 102, pp. 411-416. https://doi.org/10.1016/j.procir.2021.09.070

COMSOL, 2018. *COMSOL. Heat Transfer Module User's Guide.* COMSOL Inc., USA.

D'Addona, D.M. and Raykar, S.J. 2019. "Thermal modeling of tool temperature distribution during high-pressure coolant assisted turning". *Materials*, Vol. 12, pp. 408. https://doi.org/10.3390/ma12030408

Dourado da Silva, R.G., Ferreira, D.C., Avelar Dutra, F.V. and Lima e Silva, S.M.M. 2021. "Simultaneous real-time estimation of heat flux and hot spot temperature in machining process using infrared camera". *Case Studies in Thermal Eng.*, Vol. 28, pp. 101352. https://doi.org/10.1016/j.csite.2021.101352

Kashani, M.M., Movahhedy, M.R., Ahmadian, M..T and Razavi, R.S. 2016. "Analytical prediction of the temperature field in laser-assisted machining". In *Procedia CIRP 2016*, Vol. 46, pp. 575-578. https://doi.org/10.1016/j.procir.2016.04.071

Levenberg, K. 1944. "A method for the solution of certain non-linear problems in least squares". *Quarterly of Applied Mathematics*, Vol. 2(2), pp. 164-168. https://doi.org/10.1090/qam/10666

Lian, Y., Chen, X., Zhang, T., Liu, C., Lin. L., Lin, F., Li, Y., Chen, Y., Zhang, M. and Zhou, W. 2023. "Temperature measurement performance of thin-film thermocouple cutting tool in turning titanium alloy". *Ceram. Int*. Vol. 49, pp. 2250-2261. https://doi.org/10.1016/j.ceramint.2022.09.193

Lima e Silva, S.M.M., Brito, R.F. and Carvalho, S.R. 2015. "Experimental investigation of thermal aspects in a cutting tool using COMSOL and inverse problem". *Applied Thermal Eng.*, Vol. 85, pp. 60-68. https://doi.org/10.1016/j.applthermaleng.2015.03.083

Machado, A.R., Coelho, R.T., Abrão, A.M. and Silva, M.B. 2015. *Teoria da usinagem dos materiais*. Editora Blucher: São Paulo, Brazil.

Marquardt, D.W. 1963. "An algorithm for least-squares estimation of nonlinear parameters". *Journal of the Society for Industrial and Applied Mathematics*, Vol. 11(2), pp. 431-441. https://doi.org/10.1137/0111030

MATLAB, 2023. *Evaluate Heat Flux of Thermal Solution at Nodal or Arbitrary Spatial Locations*, 2023. https://www.mathworks.com/help/pde/ug/pde.steadystatethermalresults.evaluateheatflux.html. Accessed 19 May 2023.

Nelder, J.A. and Mead, R. 1965. "A simplex method for function minimization". *The Computer Journal*, Vol. 7(4), pp. 308-313. https://doi.org/10.1093/comjnl/7.4.308.

Nosko, O. 2024. "An inverse algorithm for contact heat conduction problems with an interfacial heat source based on a first-order thermocouple model". *Int. Comm. in Heat and Mass Transfer,* Vol. 158, pp. 107889. https://doi.org/10.1016/j.icheatmasstransfer.2024.107889

PARDISO-PROJECT, 2019. https://www.pardiso-project.org. 55.

Santos, M.R., Lima e Silva, S.M.M., Machado, A.R., Silva, M.B., Guimarães, G. and Carvalho, S.R. 2014. "Analyses of effects of cutting parameters on cutting edge temperature using inverse heat conduction technique". *Math. Problems in Eng.*, Vol. 11. http://dx.doi.org/10.1155/2014/871859.

Soler, D., Aristimuño, P.X., Saez-de-Buruaga, M., Garay, A., Arrazola, P.J. 2018. "New calibration method to measure rake face temperature of the tool during dry orthogonal cutting using thermography". *Applied Thermal Eng.*, Vol. 137, pp. 74-82. https://doi.org/10.1016/j.applthermaleng.2018.03.056

Thornton, E.A. and Wieting, A.R. 1979. "Finite element methodology for transient conduction/forced-convection thermal analysis". In *ARC – Aerospace Research Central*. https://doi.org/10.2514/6.1979-1100

Trent, E.M., Wright, P.K. and Dearnley, P.A. 2025. *Metal Cutting: Theory, Selection, and Design*. 5ª ed. Elsevier, Oxford. https://shop.elsevier.com/books/metal-cutting/trent/978-0-323-99155-1

7. RESPONSIBILITY NOTICE

The authors are the only responsible for the printed material included in this paper.